# Liquid Crystalline Phases, Microtwinning in Crystals and Helical Chirality Transformations in a Main-Chain Chiral Liquid Crystalline Polyester

**Christopher Y. Li,† Shi Jin, Xin Weng, Jason J. Ge, Dong Zhang, Feng Bai, Frank W. Harris, and Stephen Z. D. Cheng***

*Maurice Morton Institute and Department of Polymer Science, The University of Akron, Akron, Ohio 44325-3909*

**Donghang Yan and Tianbai He**

*Changchun Institute of Applied Chemistry, Chinese Academy of Science, Changchun, Jilin 130022, China*

**Bernard Lotz**

*Charles Sadron of Macromolecules, 6 Rue Boussingault, Strasbourg 67083, France*

**Liang-Chy Chien**

*Liquid Crystal Institute, Kent State University, Kent, Ohio 44010-0001*

*Received March 21, 2002; Revised Manuscript Received April 29, 2002*

ABSTRACT: A main-chain nonracemic chiral liquid crystalline polymer was synthesized from (*R*)-(−)-4′-{*ω*-[2-(*p*-hydroxy-*o*-nitrophenyloxy)-1-propyloxy]-1-decyloxy}-4-biphenylcarboxylic acid. This polymer contained 10 methylene units in each chemical repeating unit and was abbreviated PET(*R**-10). On the basis of differential scanning calorimetry, wide-angle X-ray diffraction, and polarized light microscopy experiments, chiral smectic C ($S_C$*) and chiral smectic A ($S_A$*) phases were identified. Both flat−elongated and helical lamellar crystal morphologies were observed in transmission electron microscopy. Of particular interest was the flat−elongated lamellar crystals were constructed via microtwinning of an orthorhombic cell with dimensions of $a = 1.42$ nm, $b = 1.28$ nm, and $c = 3.04$ nm. On the other hand, the helical lamellar crystals were exclusively left-handed, which was opposite to the right-handed helical crystals grown in PET(*R**-9) and PET(*R**-11) (having 9 and 11 methylene units, respectively). Note that these three polymers had identical right-handed chiral centers (*R**-). Therefore, a single methylene unit difference on the polymer backbones on an atomic length scale substantially changed the chirality of the crystals in the micrometer length scale. Furthermore, aggregates of these helical crystals in PET(*R**-10) did not generate banded spherulites in polarized light microscopy. Possible reasons for this change and loss of helical senses (handedness) on different length scales in chirality transferring processes were discussed.

## Introduction

The synthesis of asymmetric, nonracemic polymers having atomic chiral centers in their backbones has provided a unique opportunity to study new phase structures and morphologies in nano- and micrometer length scales. These materials have also initiated extensive efforts aimed at connecting synthetic chiral polymers with biopolymers and low molecular weight (MW) chiral liquid crystals.[1−3] However, it is not yet clear how these atomic chiral centers affect the chirality on larger length scales. In nonracemic chiral polymers, the understanding of chirality starts with identifying four different chiral structural hierarchies on different length scales from chemical centers to supramolecular assemblies.[4,5] For example, asymmetric chiral centers in polymer backbones, which are *primary* chiral structures (configurational chirality), usually result in helical conformations (a *secondary* chiral structure, conformational chirality). When chains with helical conformations are packed together to form ordered structures, the chirality may break local mirror symmetry and lead to a helical morphology (a *tertiary* chiral structure, phase chirality). An aggregate of multiple tertiary chiral structures, such as in the case of spherulites, forms the highest level of chiral structure (a *quaternary* chiral structure, object chirality).

Transferring chiralities from one structural level to another has been one of the key discussing topics in recent literature. However, their mechanisms have been proven to be more complicated than one would usually predict. For example, in poly(propylene oxide) (PPO), the (*R*)-(−) enantiomers generate banded spherulites that possess right-handedness while the (*L*)-(+) enantiomers generate left-handedness in their banded spherulites. However, the banded texture disappears in spherulites made up of a 50:50 mixture of (*R*)-(−)- and (*L*)-(+)-PPO enantiomers.[6] The chiral configurations in the polymer backbones (the primary chiral structure) must thus play an important role in the formation of the banded texture in spherulites (the quaternary chiral structure). In another example, the (*R*)-(−) enantiomer of poly(hydroxybutyrate) (PHB) obtained from its natural bacterial source displays a left-handed twist in the PHB banded spherulites.[7,8] In other words, opposite

* To whom correspondence should be addressed. E-mail: cheng@polymer.uakron.edu.

† Current address: Department of Materials Engineering, Drexel University, Philadelphia, PA, 19104. E-mail: chrisli@drexel.edu.

10.1021/ma0204453 CCC: $22.00 
Published on Web 06/04/2002

handedness is observed in the (*R*)-(−) enantiomers of PHB and PPO spherulites. A recent study also shows that unlike banded spherulites, lamellar single crystals of optically active (*R*)-(−)- and (*S*)-(+)-poly(epichlorohydrin) grown from solution are flat in shape.[9] The configurational and conformational chiralities are thus not transferred to the phase chirality, meaning that the chiral memory is lost after the conformational structural hierarchy.

More examples of controlling chirality can be found in biopolymers. By tuning the chirality of the residues, repeating units, side chains, and/or initiators between *dextro* and *levo*, one can obtain a single, specific handedness in a helical conformation.[10] Helical handedness can also be controlled by external environmental variables including achiral stimuli such as pH, solvent, temperature, light, and salt concentration.[11−14] For example, in certain macromolecules, chain conformations can change between plus (P) and minus (M), a so-called helix−helix transition, with only a change in temperature.[15,16]

Research on controlling chirality and chirality transfer has brought much insight into other important fields that deal with helical appearances in different length scales such as chiral liquid crystals, chiral self-assemblies, and chiral crystals. Self-assembled helical morphologies have been reported for decades.[17−20] Helical handedness changes with temperature in the cholesteric and smectic C* ($S_C$*) phases of chiral liquid crystals have also been observed, similar to the helix−helix transition of macromolecular conformation.[21] The helical morphology is often considered to be, in some ways, related to the configurational and conformational chirality on smaller length scales, although a quantitative understanding has not been achieved.[22−26]

Attempting to link the primary chiral structure with the quaternary chiral structure without knowing the secondary and tertiary chiral structures is an incomplete practice. Transferring from one chirality hierarchy to another is neither automatic nor necessary. Establishing quantitative relationships between configurational chirality and object chirality requires information on conformational and phase chiralities as well as molecular and phase structural packing schemes.[4,5] Furthermore, configurational chirality is not necessarily the only cause of lamellar twisting. Examples can be found in the twisted lamellar crystals of nonchiral polyethylene (PE)[7,27] and other polymers forming banded spherulites.[28] The twisted lamellar crystals may form due to different molecular packing and/or bending mechanisms.

We have reported on a nonracemic chiral main-chain liquid crystalline (LC) polyester synthesized from (*R*)-(−)-4′-{$\omega$-[2-(*p*-hydroxy-*o*-nitrophenyloxy)-1-propyloxy]-1-nonyloxy}-4-biphenylcarboxylic acid having nine methylene units in one chemical repeat unit. This polymer has been abbreviated as PET(*R**-9).[29] Three LC phases have been identified in PET(*R**-9): chiral smectic A ($S_A$*), twisted grain boundary smectic A (TGBA*), and $S_C$* phases.[30] Moreover, this polymer can grow flat−elongated and right-handed helical lamellar crystals from LC phases. Both of the crystals possess identical crystal structures and chain-folding directions along the long axis of the crystals, although chain orientations in these two crystal packings are different.[4,5,30−33]

To understand the effect of the number of methylene units on the phase structures and crystal morphologies, a PET(*R**-10) has been synthesized. This polymer possesses the identical configurational chiral center as PET(*R**-9) and one extra methylene unit (for a total of 10) in the backbone. In this publication, we report LC and crystalline structural identifications and phase transition behaviors of this nonracemic chiral polyester. It is intriguing that PET(*R**-10) exhibits both structural and morphological differences from PET(*R**-9) and PET(*R**-11) (having 11 methylene units). These experimental observations may serve as important evidence that helps us to achieve a better understanding of the chirality-transferring phenomenon between different length scales.

## Experiential Section

**Materials and Sample Preparation.** The PET(*R**-10) was synthesized from (*R*)-(−)-4′-{$\omega$-[2-(*p*-hydroxy-*o*-nitrophenyloxy)-1-propyloxy]-1-decyloxy}-4-biphenyl carboxylic acid. The detailed synthetic routes of the monomer and polymer were published elsewhere.[29] The polymer possessed right-hand chiral centers (*R**) along the main-chain backbone, and the number of methylene units in this polymer was 10. The chemical structure is

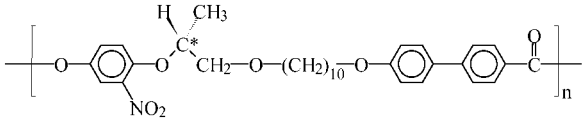

The weight-average MW was 40K and the polydispersity was 2.07, as measured by gel permeation chromatography based on polystyrene standards. A low MW sample with 10K was also synthesized.

Polymer thin films (with a thickness of 50−100 nm) were prepared via solution casting of a 0.05% (w/v) tetrahydrofuran solution on carbon-coated glass slides for transmission electron and atomic force microscopy (TEM and AFM) experiments. After the solvent was evaporated, the films were heated in a Mettler heating stage (FP-90) to 190 °C, which was above the polymers highest endothermic transition temperature for 3 min. The samples were then quenched to preset temperatures and held isothermally for various prolonged time periods ranging from one to several days. The samples were subsequently quenched into liquid nitrogen and allowed to return to room temperature (note that the glass transition temperature of this polymer was at 36 °C). The thin film samples were first examined under both polarized light (PLM) and phase contrast microscopes before they were used for AFM or shadowed by Pt and coated with carbon for TEM observations. For differential scanning calorimetry (DSC) and one-dimensional (1D) wide-angle X-ray diffraction (WAXD) measurements, thick film samples with a thickness of ∼0.1 mm were prepared. The TEM replica method was also utilized in examining surface crystalline morphology for some of these samples. Fibers were spun from the LC phase in order to determine phase structures using 2D WAXD experiments. A typical fiber diameter was 30 $\mu$m. For PLM film samples, a thickness of ∼10 $\mu$m was used by melt-pressing small amounts of samples between two glass slides.

**Equipment and Experiments.** The thermal transition behaviors were studied on a Perkin-Elmer DSC-7 instrument. The temperature and heat flow scales at different cooling and heating rates (0.5−20 °C/min) were calibrated using standard materials. The samples were first heated to above the highest transition temperature to erase the thermal history. Cooling experiments always preceded heating ones, and the cooling and heating rates used were always identical. The transition temperatures were determined by measuring onset and peak temperatures from cooling and heating scans at different rates.

1D WAXD powder experiments were performed with a Rigaku 12 kW rotating anode generator (Cu K$\alpha$ radiation) equipped with a diffractometer. A hot stage was coupled with

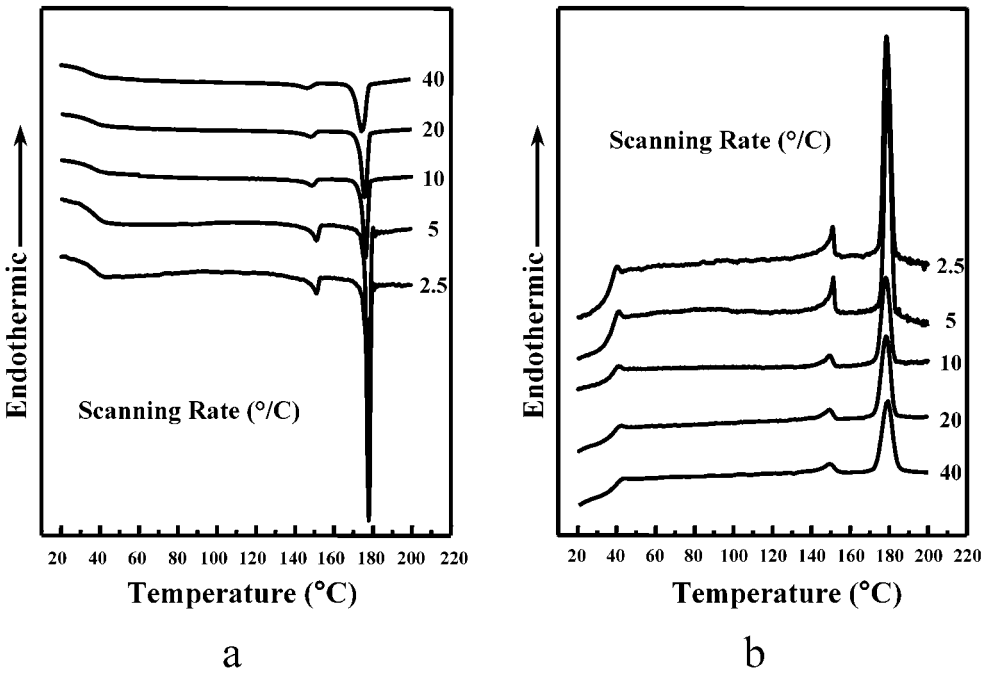


**Figure 1.** Two sets of DSC cooling and heating diagrams of PET(*R**-10) at different rates between 2.5 and 40 °C/min.

the diffractometer to study the structural evolution with temperature at constant heating and cooling rates, and the temperature was controlled to ± 1 °C. Thick films were mounted on aluminum sheets and the diffraction patterns were collected using a reflection mode. Samples were scanned in a 2$\theta$ range between 1.5 and 35°. Background scattering was subtracted from the sample diffraction patterns. 2D WAXD fiber patterns were obtained from a Rigaku X-ray imaging system with an 18 kW rotating anode X-ray generator. A hot stage was also coupled with the diffractometer. A 50-min exposure was required for a high quality WAXD fiber pattern. The background scattering was also subtracted from the fiber patterns.

Phase morphology and LC defects were examined via a PLM (Olympus BH-2) coupled with a Mettler heating stage (FP-90). Both isothermal and nonisothermal experiments were performed for PLM observations. TEM experiments were carried out in a JEOL (1200 EX II) TEM using an accelerating voltage of 120 kV. Selected area electron diffraction (SAED) patterns of the samples having different zones were obtained using a TEM tilting stage in order to determine crystal unit-cell symmetry and dimensions. Calibration of the ED spacing was done using the TlCl *d* spacings and their doublets. An AFM (Digital Instrument Nanoscope IIIA) was used to examine the PET(*R**-10) helical single-crystal morphology. The force used by the cantilever was light enough to limit damage to the sample, yet obtain accurate surface features. The scanning rate was 1−3 Hz for the low magnification images (512 × 512 pixels per image).

To study chain-folding direction of the lamellar crystals, a PE decoration method was utilized.[34,35] During the decoration, an optimal 10 cm distance between the sample and the basket was chosen in the vacuum evaporator where PE was degraded and evaporated. The samples were then treated following the procedure as described previously.

## Results and Discussion

**Thermodynamic Transition Properties and Structural Evolutions of the LC Phases.** Figure 1 shows two sets of DSC thermal diagrams at different cooling and heating rates ranging between 2.5 and 40 °C/min. A major thermal event takes place at an onset temperature of 179 °C, and a small thermal transition occurs at 151 °C. The heats of these two transitions were

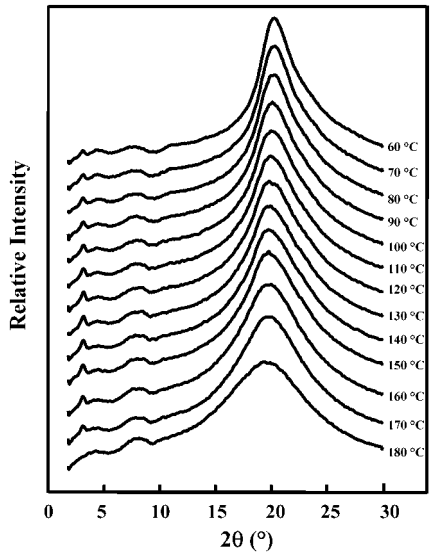


**Figure 2.** Set of WAXD powder patterns of PET(*R**-10) during cooling at 0.5 °C/min.

4.43 and 0.76 kJ/mol, respectively. Neither the onset transition temperatures nor the heats of transition exhibit much heating or cooling rate dependence. Therefore, these two transitions are identified as low ordered LC transitions.

Figure 2 shows a set of 1D WAXD patterns during cooling of PET(*R**-10) at a rate of 0.5 °C/min. The WAXD patterns during heating are identical to the results in Figure 2. The LC phase formation is signaled by a low-angle reflection (2$\theta$ = 2.91°) that appears between 170 and 180 °C. As recording WAXD patterns at a temperature interval of every 2 °C during cooling, the low-angle reflection appears between 178 and 179 °C (not shown in Figure 2). A scattering halo at 2$\theta$ = 19.4° corresponded to a liquidlike short-range order in molecular lateral packing, and it also takes a sudden but slight shift to a higher 2$\theta$ angle between 178 and 179 °C. This indicates that the high-temperature transition at 179 °C in DSC is a transition from the isotropic

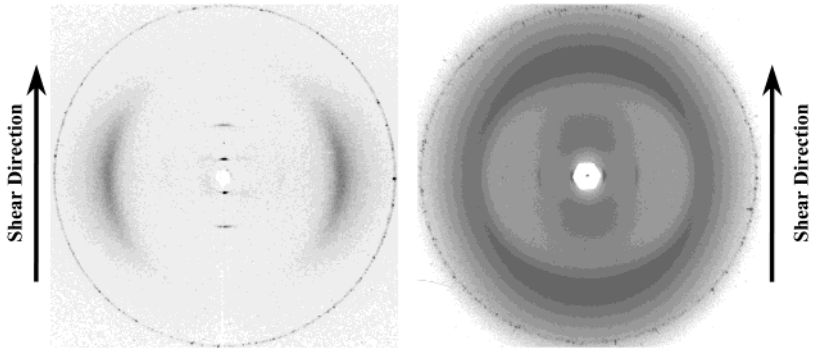


**Figure 3.** WAXD fiber patterns of the $S_A$* phase at 160 °C for the high MW PET(*R**-10) (a) and low MW PET(*R**-10) (b). The molecular chain axes are parallel to the shear direction in part a and perpendicular to the shear direction in part b.

melt (I) to a low ordered smectic phase. When the temperature is decreased to ~150 °C, the low-angle reflection in the 1D WAXD patterns shows a small but distinguishable shift toward a higher $2\theta$ angle ($d$ spacing changes from 3.04 to 2.96 nm). This shortening of the $d$ spacing at ~150 °C during cooling may be explained by molecular chain tilting to form another smectic phase (must be a $S_C$* phase). This corresponds to the DSC transition at the 151 °C observed in Figure 1 that possesses the small heat of transition.

To precisely identify the structures of these two low-ordered smectic phases, a 2D WAXD pattern of the oriented sample is taken at 160 °C as shown in Figure 3a. A pair of the low-angle layer reflections is on the meridian and the high-angle amorphous halos are on the equator. This pattern can be recognized as a $S_A$* WAXD pattern, and the molecular chains are parallel to the fiber direction. In our previous report, we found that PET(*R**-9) molecular chains were aligned perpendicular to the drawing direction.[30] This could be due to the MW effect [40K in the present study compared with the previous report of 16K in PET(*R**-9)]. Supporting evidence can be found in a 2D WAXD pattern shown in Figure 3b that is obtained from a low MW PET(*R**-10) (10K). It is indeed that the chains are perpendicular to the fiber axis. It had also been reported that the alignment of main-chain LC polymers in smectic phase depended upon the temperature of shearing, the shearing rate, and the polymers MW.[36,37] On the basis of the results of Figure 3, it is evident that the shift of the low $2\theta$ angle peak in Figure 2 is due to the chain tilting with respect to the layer normal. Therefore, the low-temperature transition at 151 °C is identified as a $S_A$* ↔ $S_C$* phase transition. These LC phase assignments can also be supported by the focal conic textures observed in PLM experiments at 160 °C as shown in Figure 4 for the $S_A$* phase. The PLM morphology of the $S_C$* phase shows little difference from that in Figure 4.

It should be noted that even when a very slow scanning rate of 0.5 °C/min is used, the high-temperature transition still remains a single peak. This differs from the transition behavior of PET(*R**-9) whose high-temperature transition peak broadened and eventually separated into two transition peaks with decreased the scanning rates.[30] This separation of the transition peak was attributed to the existence of the TGBA* phase which was between the I and the $S_A$* phases. However, in PET(*R**-10), only the I ↔ $S_A$* phase transition exists in the high-temperature region. On the other hand, no

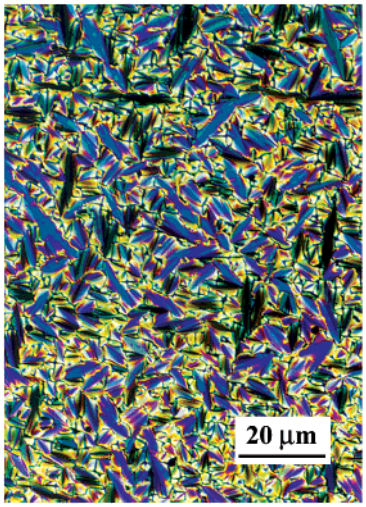


**Figure 4.** PLM LC focal conic texture of the $S_A$* phase at 160 °C.

crystallization is observed in the DSC diagrams at a cooling and heating rates of 2.5 °C/min as shown in Figure 1. This indicates that crystallization rate of PET-(*R**-10) is much slower than that of PET(*R**-9).

**Structural Determination of the Flat−Elongated Lamellar Crystals.** Lamellar crystals of PET-(*R**-10) can be grown under isothermal crystallization conditions for prolonged times to investigate the crystalline structure and lamellar crystal morphology. Figure 5a shows a TEM micrograph of a flat−elongated lamellar crystal of PET(*R**-10) grown at 130 °C for 1 day in the $S_C$* phase. The aspect ratio of the long and short axes can be as large as 40 for a well-developed lamella. An interesting feature of the crystal is the presence of cracks, all of which are along the short axis. They may have formed during quenching the crystal from 130 °C to liquid nitrogen because the coefficients of thermal expansion along both the long and short axes of the crystal may be anisotropic. This would lead to a difference of dimensional shrinkage along these two axes. Once the crystals could not sustained such a strain, cracks may form as in the case of syndiotactic polypropylene.[38,39] A PE decoration on the lamellar surface shown in Figure 5b indicates that the PE crystal rods are parallel to the short axis. Since the PE molecules are perpendicular to the long axis of the PE rods, the chain-folding direction of this flat−elongated lamellar crystal must have been along the long axis of the crystal. No sectorization is found.

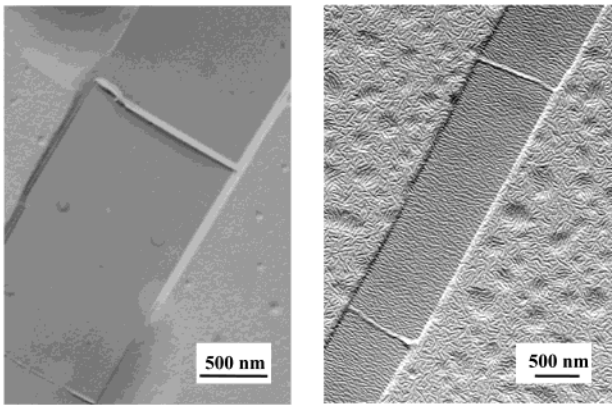


**Figure 5.** (a) Flat−elongated lamellar crystal of PET(*R**-10). (b) PE oligomer decorated flat−elongated lamellar crystal. The cracks of the lamellae may be formed during cooling due to different coefficient of thermal expansion along the long and short axes of the crystals.

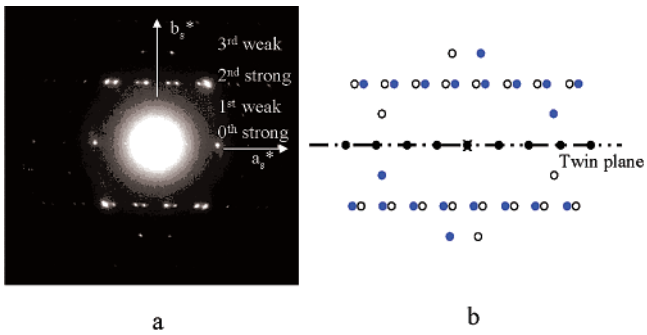


**Figure 6.** SAED pattern of a flat−elongated lamellar crystal as shown in Figure 5a (a), that can be de-convoluted into two sets of diffractions (b, open and filled circles) that are mirror images of each other. It is obviously a twin structure and the twin axis is along $a_s$*.

Figure 6a shows a SAED pattern taken from the lamellar crystal in Figure 5a. The $a_s$* and $b_s$* are defined along the horizontal and vertical axes of the pattern, respectively, which correspond to the short and the long axes of the crystal in real space (the subscript s indicates a superlattice, and see below for experimental evidence). An orthogonal lattice with two axes parallel to the $a_s$* and $b_s$* cannot, however, fit all the diffraction spots in this ED pattern. Furthermore, the weak diffraction layers parallel to the $a_s$* axis appear at the $^1/_2$ distance between the strong neighboring diffraction layers in PET(*R**-10), while they were at the $^1/_3$ distance of the strong neighboring diffraction layers in PET(*R**-9).[4,31−33] Both of them are representative of the superlattices in these two polymers.

Crystallographic analysis shows that the pattern in Figure 6a can be identified as a twin structure, and the twin plane is along the $a_s$* axis in reciprocal space as illustrated in Figure 6b. Two sets of the ED spots are represented by the open and filled circles, respectively, and these two ED patterns are identical and fit in a 2D rectangular lattice. By applying a mirror operation along the $a_s$* axis, the open circle spots can be converted to the filled circle ones, and vice versa. This can be confirmed by the long-time exposed ED pattern shown in Figure 7. More than 300 diffraction spots are identified in this pattern, and they can be separated into two ED sets that share the mirror plane along the $a_s$* axis.

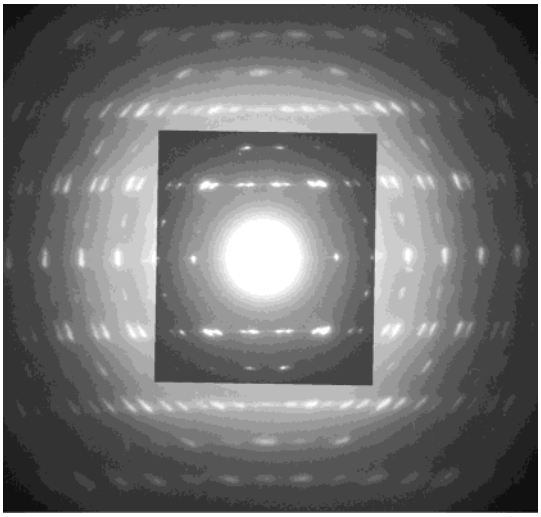

**Figure 7.** Long time exposed SAED pattern of a PET(*R**-10) single crystal. The inset is the pattern shown in Figure 6a.

This twin-structural identification is further supported by SAED patterns obtained on the single crystals of PET(*R**-10) formed after the samples were mechanically sheared at 130 °C as shown in Figure 8a. Figure 8b is a corresponding SAED pattern. It is obvious that the crystal habit changed from an elongated shape to a polygonal with well-defined angles of ∼132° between the (110) and (200) edges (see Figure 8a). The SAED pattern in Figure 8b exhibits a typical orthogonal lattice with the $a_b$* and $b_b$* axes of the reciprocal lattice assigned along the horizontal and vertical directions, respectively (the subscript b represents "basic"). Therefore, the $(200)_b$ and $(110)_b$ diffractions are assigned as indicated in the figure. This 2D lattice is determined to have $a = 0.71$ nm and $b = 0.64$ nm. If a $(110)_b$ twin is constructed using this basic unit cell dimension, all the diffraction spots generated can fit into the ED pattern as shown in Figures 6 and 7. However, the periodicity of the diffraction pattern in Figure 8b is twice as much along both the $a_s$* and $b_s$* axes as it is in the diffraction pattern in Figure 6b. This suggests that that the unit cell dimensions of the basic structure have to be doubled in both *a* and *b* directions in order to construct the twined crystal (the superlattice). Therefore, the superlattice can be obtained by the (110) twin of an orthogonal cell with $a = 1.42$ nm and $b = 1.28$ nm. The fold direction in the flat−elongated lamellar crystal is along the $(110)_b$ planes defined by the basic unit cell.

Tilting experiments were conducted in order to determine the crystal *c* axis. Figure 9 shows four ED patterns having different diffraction zones by tilting around the $a_s$* axis [the $(110)_b$ reciprocal vector]. The crystal *c* axis was determined to be 3.04 nm, and it is perpendicular to the $a_s$* and the $b_s$* axes. Therefore, the unit cell, which constructs the superlattice (the twined crystal), is orthorhombic. It is interesting to note that the *c*-dimension of the PET(*R**-10) unit cell is one chemical repeat unit in length while the *c*-dimension is double of the chemical repeat unit length in PET(*R**-9).[4,31−33] This reveals that there is a difference in conformations between these two polymer crystals due to the number of methylene units (9 vs 10) in the repeating units.

It is intriguing that the structure of the flat−elongated lamellar crystal of PET(*R**-10) shown in Figure 5 is constructed by a microtwinning (or even

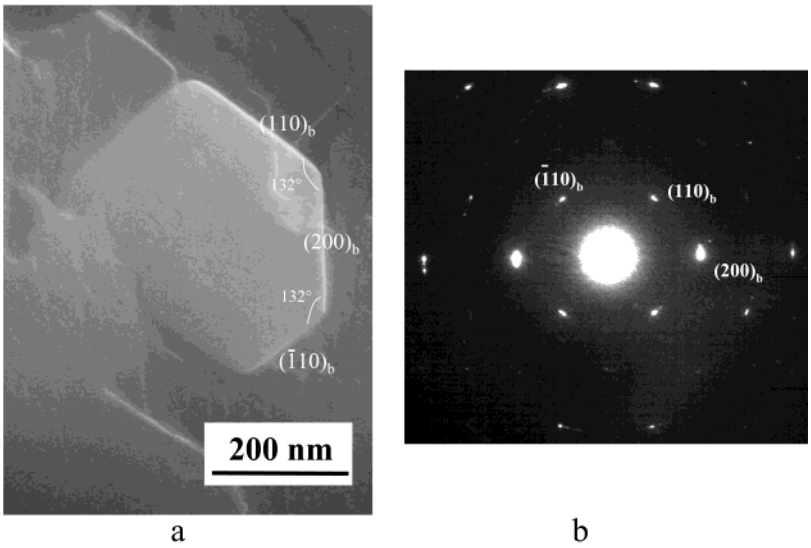


**Figure 8.** Sheared grown PET(*R**-10) single crystals (a) and their corresponding diffraction pattern (b).

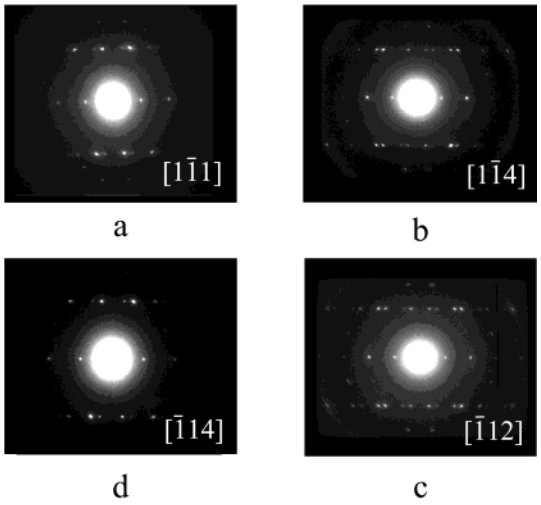


**Figure 9.** Set of tilted SAED patterns obtained by tilting around $a_s$*. Different zones can be calculated from the basic structure: (a) $[1\bar{1}1]$; (b) $[1\bar{1}4]$; (c) $[\bar{1}12]$; (d) $[\bar{1}14]$.

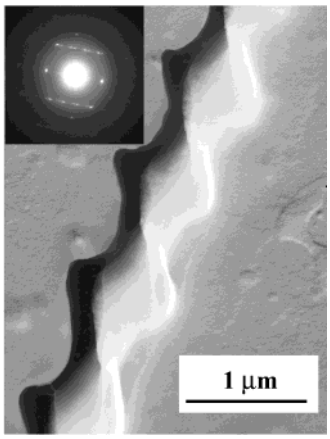


**Figure 10.** TEM micrograph of a helical single lamellar crystal of PET(*R**-10). The inset is the SAED pattern of the helical crystal with the correct orientation.

molecular-twinning) of the two identical orthorhombic lattices having the $(110)_b$ twin planes that are parallel to the long axis of the lamellar crystal. Furthermore, this lamellar habit is most frequently observed in thin-film crystallization as opposed to the polygonal-shaped crystal obtained in the mechanically sheared samples (Figure 8a). This indicates that the twin structure is possibly a favorable packing arrangement in the crystal growth. Although the ED pattern can be explained using the twinning concept, the detailed twin-packing scheme and the origin of how the doubling of the basic cell occurs are still not fully understood. We are seeking answers to these questions by exploring PET(*R**-$n$ = 7−11) homologues and using a computer simulation technique.

**Transferring Chirality in Helical Lamellar Crystals.** Helical lamellar crystals are also grown in the same crystallization condition (isothermal crystallization at 130 °C for 1 day in the $S_C$* phase) as shown in Figure 10. The pitch length of the crystal is about 2 $\mu$m in this figure. Decorated PE crystal rods on the helical lamellar crystal surface are perpendicular to the long helical axis, indicating that the chain-folding direction is also along the long axis of the crystal, which is along the $(110)_b$ planes. The insert SAED pattern of Figure 10 is obtained from the helical crystal, indicating that the helical crystals also possesses twinned orthorhombic cells that are identical to the flat−elongated crystals. The molecular orientation in the helical crystals is continuously twisted along both the $a_s$* and $b_s$* axes of the crystal.[4,33]

The most surprising phenomenon observed in Figures 10 is that the helix was *left-handed* instead of *right-handed* as shown in PET(*R**-9) and PET(*R**-11).[40] The left-handed helicity is also confirmed by AFM as shown in Figure 11 when the crystal was formed at 120 °C. On the basis of the concept of the four chirality levels described,[4,5] the helical crystals belong to the third-level chirality as shown in Figure 12.[40] Our understanding is that the molecular interaction and packing scheme rather than the lower-level chirality itself determined the next level chirality. This has been supported by observations in other chiral systems. For example, different conformational chiralities (P or M) have been observed in different environments for the same materials.[11−16] It has also been reported that a copolymer consisting of 56% (*R*)- and 44% (*L*)-polyisocyanates possesses the same helical conformation as the (*R*)-polyisocyanate homopolymer. This indicates that the *L*-enantiomer in the copolymer is forced to adopt the same conformation as that of the *R*-enatiomers.[41,42] In

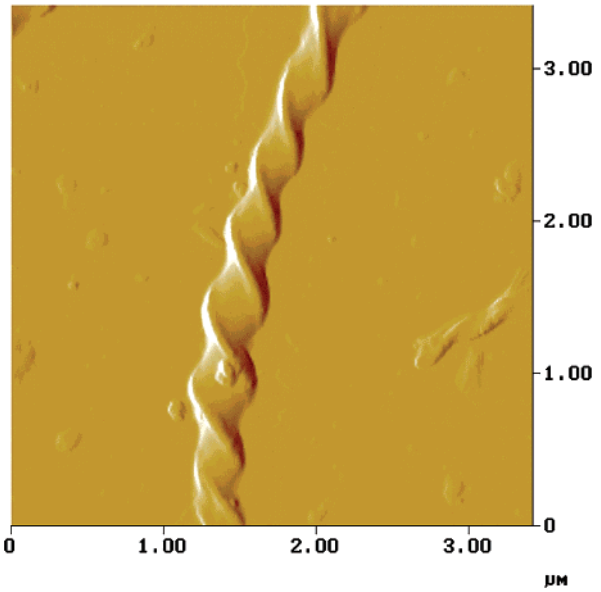


**Figure 11.** AFM tapping mode image of a helical single lamellar crystal of PET(*R**-10) isothermally formed at 120 °C.

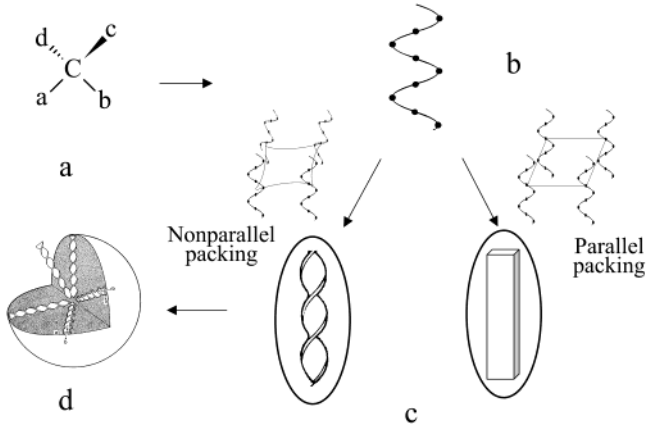


**Figure 12.** Schematic drawing of four levels of chiralities and their transferring process. The four levels of chiralities are configuration (a), conformation (b), phase (c), and object (d). The packing mechanism is the key for the higher-level chirality formation. Parallel packing of the helical chain could lead to a flat morphology while twist-packing will lead to a helical morphology. The handedness of the helicity depends on how the molecules pack together.

the present case, the molecular packing scheme has to be essential in the formation of third-level chiral structure. Helical lamellar crystals of PET(*R**-*n*) may be right-handed, left-handed, or even flat depending upon their packing schemes, even though these polymers possess the identical *R*-chiral center at the configurational level. This understanding is also supported by the chiral LC phased observed in achiral banana-shaped liquid crystals.[43−45] In these liquid crystals, molecules do not have chiral centers and are achiral on the level of configurational structure. However, helical morphology, ferroelectric properties, and the third-level (phase) chirality have been observed due to the bent mesogen cores that gave rise to the spontaneous polar symmetry-breaking in an electric field. Therefore, banana-shaped liquid crystals provide excellent examples in which the molecular packing is one of the most important steps in the formation of the third-level chirality. A more challenging topic involves explaining how one methylene unit difference alters the handedness in the helical crystals. This topic is currently under investigation.

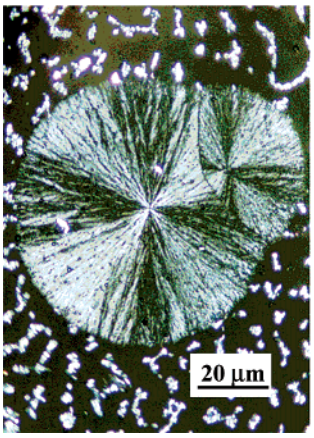


**Figure 13.** PLM micrograph of a low MW spherulite of PET-(*R**-10) grown from the melt at 130 °C.

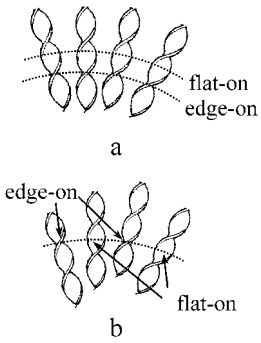


**Figure 14.** Schematic drawing of packing schemes of helical lamellar crystal to form spherulites with (a) and without (b) band texture. In part a, helical crystals are "in phase"; at the growth front, all the lamellar crystals twist to the same degree. In part b, however, helical crystals are "out of phase"; different degrees of twisting can be observed along the same spherulite growth front. Dotted lines in the figure are drawn to represent the spherulite growth fronts at different growth stages.

The formation of polymer spherulites also represents a chirality transferring process between the phase (tertiary) and object (quaternary) structural levels. Figure 13 is a PLM picture of the low MW PET(*R**-10) spherulite grown from a relatively thick sample at 130 °C. One notable feature is that the spherulite does not exhibit the banded texture. This is intriguing since the banded texture is linked to the lamellar twist. Figure 14a shows the commonly understood mechanism of the band texture in polymer spherulites. The helical lamellar crystals changing from the edge-on to the flat-on arrangements vary their overall birefringence due to different refractive indices along the three (sometimes two) crystal axes. When stacks of lamellar crystals cooperatively twist, edge-on, and flat-on arrangements along the spherulite radial direction result in alternating dark and bright bands being formed. However, Figure 14b shows a noncooperative packing scheme of the helical lamellar crystals. Although the birefringence differences of each individual lamella still exist, they aggregated together noncooperatively along the radial direction to be "out of phase". Therefore, the banded texture cannot be observed. This argument is supported by the observation of a "precursor" spherulite of low MW PET(*R**-10) using the replica method in TEM as shown in Figure 15. The helical crystals are indeed packed in a noncooperative fashion. Therefore, the absence of

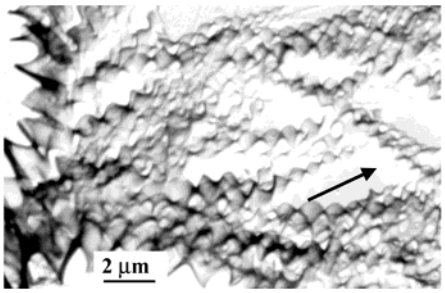


**Figure 15.** TEM morphology of a low MW PER(*R**-10) spheruliute observed via the replica method. It can be considered as a "precursors" of the spherulite shown in Figure 13. The arrow represents the growth direction of this spherulite.

macroscopic chirality (the banded texture) is a natural consequence of the chirality being "lost" during the transfer from individual lamella to a spherulite simply because of the noncooperative lamellar packing.

## Conclusion

In summary, phase structures and transition behaviors of PET(*R**-10) have been investigated. This chiral polymer exhibits the $S_A$*, and the $S_C$* LC phases. Flat−elongated lamellar crystals have also been observed in PET(*R**-10) after prolonged crystallization times at 130 °C in the $S_C$* phase. The lamellae are constructed by a microtwinning of two sets of orthorhombic unit cells having dimensions of $a = 1.42$ nm, $b = 1.28$ nm, and $c = 3.04$ nm. Helical lamellar crystals are also formed under the same crystallization conditions. The most intriguing observation about the helical lamellar crystal of PET(*R**-10) is the opposite handedness (left-handed) with respect to PET(*R**-9) and PET(*R**-11) (right-handed) even though they have the identical chiral center (*R**-). The opposite handedness of these helical crystals suggests that the molecular packing scheme plays a major role in forming the third-level phase chirality. In crystal aggregates on the fourth-level (object) chirality, PET(*R**-10) grows spherulites absent of banded texture even though the individual helical lamellar crystals are the building blocks of the spherulite. This is possibly due to the fact that the helical lamellar crystals are packed in a noncooperative way. The packing scheme, which is independent of length scale, does plays a major role in the chirality transfer process.

**Acknowledgment.** This work was supported by the NSF (DMR-96-17030) and the ALCOM Scientific and Technology Center (DMR-91-57738) at Kent State University, Case Western Reserve University, and the University of Akron.

## References and Notes

(1) Okamoto, Y.; Nakano, T. *Chem. Rev.* **1994**, *94*, 349.
(2) Special issue on Enantioselective Synthesis: *Chem. Rev.* **1992**, *92*, 739.
(3) Rowan, A. E.; Nolte, R. J. M. *Angew. Chem., Int. Ed. Engl.* **1998**, *37*, 63.
(4) Li, C. Y.; Cheng, S. Z. D.; Ge, J. J.; Bai, F.; Zhang, J. Z.; Mann, I. K.; Chien, L. C.; Harris, F. W.; Lotz, B. *J. Am. Chem. Soc.* **2000**, *122*, 72.
(5) Li, C. Y.; Ge, J. J.; Bai, F.; Calhoun, B. H.; Harris, F. W.; Cheng, S. Z. D.; Chien, L. C.; Lotz, B.; Keith, H. D. *Macromolecules* **2001**, *34*, 3634.
(6) Singfield, K. L.; Hobbs, J. K.; Keller, A. *J. Cryst. Growth* **1998**, *183*, 683.
(7) Keith, H. D.; Padden, Jr. F. *Macromolecules* **1996**, *29*, 7776.
(8) Barham, P. J.; Keller, A.; Otun, E. L.; Holmes, P. A. *J. Mater. Sci.* **1984**, *19*, 2781.
(9) Saracovan, I.; Cox, J. K.; Revol, J.-F.; Manley, R. St. J.; Brown, G. R. *Macromolecules* **1999**, *32*, 717.
(10) Fujiki, M. *J. Am. Chem. Soc.* **2000**, *122*, 3336.
(11) Nelson, J. C.; Saven, J. G.; Moore, J. S.; Wolynes, P. G. *Science* **1997**, *277*, 1793.
(12) Prince, R. B.; Saven, J. G.; Wolynes, P. G.; Moore, J. S. *J. Am. Chem. Soc.* **1999**, *121*, 3114.
(13) Blout, E. R.; Carver, J. P.; Gross, J. *J. Am. Chem. Soc.* **1963**, *85*, 644.
(14) Yashima, E.; Maeda, Y.; Okamoto, Y. *J. Am. Chem. Soc.* **1998**, *120*, 8895.
(15) Watanabe, J.; Okamoto, S.; Satoh, K.; Sakajiri, K.; Furuya, H. *Macromolecules* **1996**, *29*, 7084.
(16) Cheon, K. S.; Selinger, J. V.; Green, M. M. *Angew. Chem., Int. Ed.* **2000**, *39*, 1482.
(17) Rybnikar, F.; Geil, P. H. *Biopolymers* **1972**, *11*, 271.
(18) Keller, A.; Wills, H. H. *J. Polym. Sci.* **1959**, *39*, 151.
(19) Saupe, A. *Angew. Chem., Int. Ed. Engl.* **1968**, *7*, 97.
(20) Goodby, J. W.; Waugh, M. A.; Stein, S. M.; Chin, E.; Pindak, R.; Patel, J. S. *Nature* **1989**, *337*, 449.
(21) Kaspar, M.; Gorecka, E.; Sverenyak, H.; Hamplova, V.; Glogarova, M.; Pakhomov, S. A. *Liq. Cryst.* **1995**, *19*, 589.
(22) Fuhrhop, J. H.; Helfrich, W. *Chem. Rev.* **1993**, *93*, 1565 and references therein.
(23) Sakurai, I.; Karvamura, T.; Dakurai, A.; Kegami, A.; Setoi, T. *Mol. Cryst. Liq. Cryst.* **1985**, *130*, 203.
(24) Nandi, N.; Bagchi, B. *J. Am. Chem. Soc.* **1996**, *118*, 11208.
(25) Nandi, N.; Bagchi, B. *J. Phys. Chem. A* **1997**, *101*, 1343.
(26) Kruger, P.; Losche, M. *Phys. Rev. E*: *Stat. Phys., Plasmas, Fluids, Relat. Interdiscip. Top.* **2000**, *62*, 7031.
(27) Keith, H. D.; Padden, Jr. F.; Lotz, B.; Wittmann, J. C. *Macromolecules* **1989**, 22, 2230.
(28) Keller, A.; Wills, H. H. *J. Polym. Sci.* **1959**, *39*, 151.
(29) Bai, F.; Chien, L. C.; Li, C. Y.; Cheng, S. Z. D.; Percheck, R. *Chem. Mater.* **1999**, *11*, 1666.
(30) Li, C. Y.; Ge, J. J.; Bai, F.; Zhang, J. Z.; Calhoun, B. H.; Chien, L. C.; Harris, F. W.; Cheng, S. Z. D. *Polymer* **2000**, *41*, 8953.
(31) Li, C. Y.; Yan, D.; Cheng, S. Z. D.; Bai, F.; Ge; J. J.; He, T.; Chien, L. C.; Harris, F. W.; Lotz, B. *Macromolecules* **1999**, *32*, 524.
(32) Li, C. Y.; Yan, D.; Cheng, S. Z. D.; Bai, F.; Ge, J. J.; He, T.; Chien, L. C.; Harris, F. W.; Lotz, B. *Phys. Rev. B* **1999**, *60*, 12675.
(33) Li, C. Y.; Cheng, S. Z. D.; Ge, J. J.; Bai, F.; Zhang, J. Z.; Mann, I. K.; Harris, F. W.; Chien, L. C.; Yan, D.; He, T.; Lotz, B. *Phys. Rev. Lett.* **1999**, *83*, 4558.
(34) Wittmann, J. C.; Lotz, B. *Makromol. Rapid Commun.* **1982**, *3*, 733.
(35) Wittmann, J. C.; Lotz, B. *J. Polym. Sci., Polym. Phys. Ed.* **1985**, *23*, 205.
(36) Leland, M.; Zhang, A.; Ho, R. M.; Cheng, S. Z. D.; Keller, A.; Kricheldorf, H. R. *Macromolecules* **1997**, *30*, 5249.
(37) Romouribe, A.; Windle, A. H. *Macromolecules* **1993**, *26*, 7100.
(38) Lovinger, A. J.; Lotz, B.; Davis, D. D.; Schumacher, M. *Macromolecules* **1994**, *27*, 6603.
(39) Rodriguez-Arnold, J.; Bu, Z.; Cheng, S. Z. D.; Hsieh, E. T.; Johnson, T. W.; Geerts, R. G. Palackal, S. J.; Hawley, G. R.; Welch, B. *Polymer* **1994**, *35*, 5194.
(40) Li, C. Y.; Cheng, S. Z. D.; Ge, J. J.; Bai, F.; Zhang, J. Z.; Mann, I. K.; Harris, F. W.; Chien, L.-C.; Lotz, B. *J. Am. Chem. Soc.* **2001**, *123*, 2462.
(41) Green, M. M.; Garetz, B. A.; Munoz, B.; Chang, H. *J. Am. Chem. Soc.* **1995**, *117*, 4181.
(42) Green, M. M.; Peterson, N. C.; Sato, T.; Teramoto, A.; Cook, R.; Lifson, S. *Science* **1995**, *268*, 1860.
(43) Niori, T.; Sekine, T.; Watanabe, J.; Furukawa, T.; Takezoe, H. *J. Mater. Chem.* **1996**, *6*, 1231.
(44) Link, D. R.; Natale, G.; Shao, R.; Maclennan, J. E.; Clark, N. A.; Krblova, E.; Walba, D. M. *Science* **1997**, *278*, 1924.
(45) Heppke, G.; Moro, D. *Science* **1998**, *279*, 1872.

MA0204453